Effect of Mutation at Valine 61 on the Three-Dimensional Structure, Stability, and Redox Potential of Cytochrome b_5[†,⊥]

Lin-Long Xue,[‡,§] Yun-Hua Wang,[‡] Yi Xie,[∥] Ping Yao,[∥] Wen-Hu Wang,[‡] Wen Qian,[‡] and Zhong-Xian Huang*[,‡]

Chemistry Department and Genetic Institute, Fudan University, Shanghai 200433, PRC

Jian Wu[§] and Zong-Xiang Xia*

Shanghai Institute of Organic Chemistry, Chinese Academy of Sciences, Shanghai 200032, PRC

Received April 19, 1999; Revised Manuscript Received June 16, 1999

ABSTRACT: To elucidate the role played by Val61 of cytochrome b_5, this residue of the tryptic fragment of bovine liver cytochrome b_5 was chosen for replacement with tyrosine (Val61Tyr), histidine (Val61His), glutamic acid (Val61Glu), and lysine (Val61Lys) by means of site-directed mutagenesis. The mutants Val61Tyr, Val61Glu, Val61His, and Val61Lys exhibit electronic spectra identical to that of the wild type, suggesting that mutation at Val61 did not affect the overall protein structure significantly. The redox potentials determined by differential pulse voltammetry were −10 (wild type), −25 (Val61Glu), −33 (Val61Tyr), 12 (Val61His), and 17 mV (Val61Lys) versus NHE. The thermal stabilities and urea-mediated denaturation of wild-type cytochrome b_5 and its mutants were in the following order: wild type > Val61Glu > Val61Tyr > Val61His > Val61Lys. The kinetics of denaturation of cytochrome b_5 by urea was also analyzed. The first-order rate constants of heme transfer between cytochrome b_5 and apomyoglobin at 20 ± 0.2 °C were 0.25 ± 0.01 (wild type), 0.42 ± 0.02 (Val61Tyr), 0.93 ± 0.04 (Val61Glu), 2.88 ± 0.01 (Val61His), and 3.88 ± 0.02 h^{-1} (Val61Lys). The crystal structure of Val61His was determined using the molecular replacement method and refined at 2.1 Å resolution, showing that the imidazole side chain of His61 points away from the heme-binding pocket and extends into the solvent, the coordination distances from Fe to NE2 atoms of two axial ligands are approximately 0.6 Å longer than the reported value, and the hydrogen bond network involving Val61, the heme propionates, and three water molecules no longer exists. We conclude that the conserved residue Val61 is located at one of the key positions, the "electrostatic potential" around the heme-exposed area and the hydrophobicity of the heme pocket are determinant factors modulating the redox potential of cytochrome b_5, and the hydrogen bond network around the exposed heme edge is also an important factor affecting the heme stability.

Cytochrome b_5 is a membrane protein. It functions as an electron carrier, participating in a series of electron-transfer processes in biological systems, including reduction of ferric myoglobin (*1*), fatty acid denaturation (*2*), and the cytochrome P450 catalytic cycle (*3*). Cytochrome b_5 consists of two domains, a hydrophilic heme-containing domain and a hydrophobic one, which anchors the protein to the membrane (*4*). Proteolysis of bovine liver microsomal cytochrome b_5 by lipase produces a hydrophilic heme-containing domain consisting of 93 amino acid residues (Ser1−Ser93), which is termed cytochrome Lb_5. The three-dimensional structure of cytochrome Lb_5 was determined and refined at high resolution (*5*−*7*), which reveals that the heme iron is ligated, in a hydrophobic pocket, by His39 and His63, complemented by four N_ϵ of pyrrols of the porphyrin. When the microsomal cytochrome b_5 is treated with trypsin, a heme-containing 84-residue (Ala3−Lys86) fragment is obtained (*4*) and termed cytochrome Tb_5, and its crystal structure has not been reported yet. The crystal structure of the soluble fragment of mitochondrial cytochrome b_5 at medium resolution was recently reported (*8*), showing that its overall structure is similar to that of cytochrome Lb_5.

In the past decade, several papers were published concerning the investigation of the effects of the specific side chain of cytochrome b_5 on its structure and properties by using chemical modification (*9*) and site-directed mutagenesis (*10*−*15*). Among these, the binding and electron transfer between cytochrome b_5 and cytochrome *c* were intensively studied. On the basis of the crystal structures of cytochrome b_5 and cytochrome *c*, several computer simulation models of the complexes between cytochrome b_5 and cytochrome *c* were proposed, and the most important one is the electrostatic model (*16*, *17*), which emphasizes the role of negatively charged residues of cytochrome b_5 in the formation of the cytochrome b_5−cytochrome *c* complex.

[†] This research was supported by the National Science Foundation of China, the State Key Laboratory of Genetic Engineering of Fudan University, and the State Key Laboratory of Bio-organic and Natural Product Chemistry of the Shanghai Institute of Organic Chemistry. A grant from the National Program of Space Application is acknowledged.

[⊥] Crystallographic coordinates have been deposited in the Bookhaven Protein Data Bank under file name 1QDX.

* Corresponding authors. Telephone: +86-21-65643973. Fax: +86-21-65641740. E-mail: zxhuang@fudan.edu.cn.

[‡] Chemistry Department, Fudan University.

[§] These authors made the equal contributions to this work.

[∥] Genetic Institute, Fudan University.

10.1021/bi990893b CCC: $18.00
Published on Web 08/21/1999

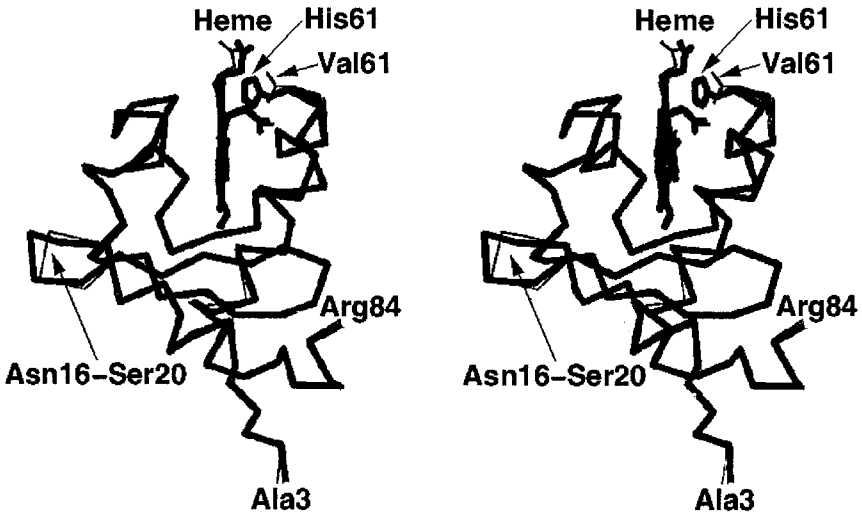

FIGURE 1: Stereoscopic C_α drawing of cytochrome Tb_5 Val61His superimposed with that of cytochrome Lb_5 (the C-terminal segment beyond Arg84 of cytochrome Lb_5 is omitted). Val61His is shown as a thick line and cytochrome Lb_5 as a thin line. Heme and the side chains of residue 61 are shown (only one of the two conformations of Val61 of cytochrome Lb_5 is shown). Ala3, Arg84, and the segment of Asn16−Ser20 are denoted. This diagram was prepared using the molecular graphics software SETOR (*72*).

Studying the contribution of individual amino acids to the properties and functions of a specific protein is a challenge. In the previous studies on the relationship between the structure and properties of cytochrome b_5, the main efforts were focused on investigating the roles of two types of conserved residues. One is the axial ligation residues, His39 and His63 (*18*, *19*). The other type is the negatively charged residues thought to be involved in the formation of the complex of cytochrome b_5 and its binding partners (*10*, *20*−*24*). It was concluded that the critical amino acids making important contribution to the protein stability are relatively rigid or buried in the folded structure (*11*, *25*, *26*). However, a number of studies revealed that the noncharged residues around the heme-exposed edge region of cytochrome b_5 also played an important role in modulating the redox potential, maintaining the heme stability, and binding to its partners. Valine 61 of cytochrome b_5, located at the rim of the hydrophobic pocket and near the iron ion of the heme (Figure 1), is one of these residues at a critical position of this region. Val61 is also a residue of cytochrome b_5 conserved in most species with the only exception being horse (*4*). It is suggested that Val61 is involved in the hydrophobic interaction at the interface between cytochrome b_5 and cytochrome *c* (*27*). To provide further insight into the role of Val61, a combination of genetic, thermodynamic, and structural data will be most useful for estimating its specific contribution to the protein properties and functions. Therefore, we have constructed four mutants of cytochrome b_5 to study the effects of the polarity, electric charge, and volume of the substituted residues on the three-dimensional structure, stability, and redox potential of the protein. The relatively small and nonpolar residue Val61 was replaced, using site-directed mutagenesis, with large and charged or polar residues, glutamic acid (Val61Glu), tyrosine (Val61Tyr), histidine (Val61His), and lysine (Val61Lys). Herein, we report the characterization of cytochrome b_5 variants by ES-MS (electrospray mass spectrometry), electronic spectra, and redox potential measurements. The three-dimensional structure of one of the mutants, Val61His, at 2.1 Å resolution is also presented in this paper, which was determined by X-ray analysis. The heme stability of the purified mutants of cytochrome b_5 was examined by denaturation and heme transfer reaction between cytochrome b_5 and apomyoglobin. The effects of the mutation at Val61 on the crystal structure, stability, and redox potential are discussed.

MATERIALS AND METHODS

Materials. All endonucleases were purchased from Biolabs. X-gal and IPTG were purchased from Sigma. [α-^{32}P]-dCTP and [γ-^{32}P]dATP were obtained from Amersham. All chemicals were reagent grade. The synthesized gene encoding tryptic bovine hepatic cytochrome b_5 was a gift from M. R. Mauk (*28*). Myoglobin was obtained from Sigma, and apomyoglobin was prepared according to the published method (*29*).

Mutagenesis, Expression, and Purification of Cytochrome b_5. The single-site mutations were accomplished according to the method of Zoller and Smith (*30*). Four 21-base oligonucleotides were synthesized, and the codon of Val61 (GTT) was changed into CAT (His), AAG (Lys), TAC (Tyr), and GAA (Glu). The mutant genes from M13mp18 RF DNA were cloned into the *Eco*RI−*Hin*dIII-cut pUC19 plasmid and then transformed into *Escherichia coli* JM83 cells. The expression and purification of mutant cytochrome b_5 were carried out according to the method of Mauk (*14*). The ratios of the absorbance at 412 nm to that at 280 nm of wild-type cytochrome b_5 and its four mutants were all above 5.7, suggesting that the purity of the protein is high enough for further analysis.

Electrospray Mass Spectrometry. Electrospray mass spectrometry (ES-MS) was performed on a Quattro MS/MS system (VG Co.) equipped with an electrospray ionization system (Analytic Co.). The protein was dissolved in a methanol solution (10%). The final concentration of cytochrome b_5 was 20 mM.

UV−Visible Spectrometry. Electronic spectra were recorded on a Hewlett-Packard 8452A diode array spectrometer. The protein was dissolved in phosphate buffer (pH 7.0, 100 mM) with a concentration of around 10 mM. The reduced protein was prepared by addition of a small amount of sodium dithionite (*31*).

Redox Potential. The redox potentials were measured by differential pulse voltammetry. Experiments were performed at 25 ± 1 °C using a PAR M273 Potentat Galvanostate (Princeton, NJ) which was interfaced with an IBM computer and controlled by PAR M270 software. The cell consists of a conventional three-electrode system with a small volume sample ($V \sim 0.5$ mL). The working electrode was a 2 mm diameter gold disk electrode, with a platinum wire coil as the counter electrode and a Ag/AgCl/KCl (3 M) electrode as a reference electrode. The pulse height is 10 mV, and its width is 50×10^{-3} s. The scan rate is 1 mV/s. The polishing and modification of the working electrode were accomplished according to the published method (*32*).

Thermal Denaturation. For thermal denaturation of the wild type and variants of cytochrome b_5, the protein concentration was about 10 mM in phosphate buffer (pH 7.0, 100 mM). The change in optical absorption at the Soret band was measured with a Hewlett-Packard 8452A diode array spectrophotometer. Experiments were carried out over a temperature range of 25−85 °C. The temperature was directly determined in the cuvette holder and was maintained within ±0.2 °C for 15 min to ensure that the samples reached equilibrium.

Urea-Mediated Denaturation of Cytochrome b_5. To assess the urea-mediated denaturation of cytochrome b_5, the absorbance at 412 nm was monitored after 0.3 mL of cytochrome b_5 (phosphate buffer, pH 7.0, 100 mM) and 2.7 mL of urea (phosphate buffer, pH 7.0, 100 mM) had been mixed for 18 h at 30 °C. The final concentration of cytochrome b_5 was 4 mM, and the concentration of urea varied from 0 to 9 mol/L. For the kinetic study of urea-mediated denaturation of cytochrome b_5, the time course of the absorbance increase at 412 nm was recorded immediately after the two solutions were mixed. All measurements were carried out on a 8452A diode spectrophotometer (Hewlett-Packard).

Heme Transfer Kinetics. The kinetics of heme transfer between cytochrome b_5 and apomyoglobin were determined on a Hewlett-Packard 8452A diode array spectrophotometer. A tandem cuvette holder was employed to hold the solutions of apomyoglobin and cytochrome b_5. Immediately after the mixing of apomyoglobin and cytochrome b_5, the time courses of the absorption at 406 nm, corresponding to the maximum of the difference spectra between cytochrome b_5 and myoglobin, were recorded spectroscopically at 20 ± 0.2 °C. The final concentrations of apomyoglobin and cytochrome b_5 were both 5 mM based on weighting.

Analysis of Denaturation Curves. (1) Equilibrium Study. The process of denaturation of cytochrome b_5 by heat or urea is thought to be a procedure of heme dissociation from the holoprotein and can be described by a two-state mechanism (*33*, *12*)

$$\mathrm{H} \Leftrightarrow \mathrm{A} \tag{1}$$

in which H represents the holoprotein and A the apoprotein. The equilibrium constant K_D can be calculated from

$$K_D = f_A/f_H = (A_H - A_{412})/(A_{412} - A_A) \tag{2}$$

where A_A and A_H and f_A and f_H are the absorptions and fractions of cytochrome b_5 in the apo and holo forms, respectively. K_D is related to the free energy of the heme dissociation ΔG_D

$$\Delta G_D = -RT \ln K_D \tag{3}$$

The free energy of the heme dissociation, at room temperature and zero urea concentration, can be estimated by linear extrapolation and fits the following equation:

$$\Delta G_D = \Delta G_D{}^0 - m_D[\text{denaturant}] \tag{4}$$

where [denaturant] is the concentration of urea or the temperature (T in kelvin) and m_D is the slope of the plot of ΔG_D versus temperature or urea concentration. The difference in free energy between the wild type and the mutants can be estimated from

$$\Delta(\Delta G_D{}^0) = \Delta G_D{}^0{}_{WT} - \Delta G_D{}^0{}_{mutant} \tag{5}$$

Since the linear extrapolation under nondenaturing conditions according to the above equation could give rise to 30% error (*12*), the $\Delta(\Delta G_D°)$ was usually estimated at the midpoint of heme dissociation

$$\Delta(\Delta G_D{}^{50\%}) = \langle m \rangle[(\text{denaturant})_{(WT)}{}^{50\%} - (\text{denaturant})_{(mutant)}{}^{50\%}] \tag{6}$$

where $(\text{denaturant})^{50\%}$ are the midpoint values of heme dissociation and $\langle m \rangle$ is the average of the m_D values, for the wild type and the mutant proteins.

(2) Kinetic Studies. The kinetics of heme dissociation from cytochrome b_5 by urea were analyzed as described in the literature (*12*, *34*). The free energy of activation of heme dissociation ΔG^{1D} can be derived from the following equation:

$$\Delta G_D{}^{\neq} = -RT \ln(hk_D/k_BT) \tag{7}$$

where R is the gas constant, T the absolute temperature, h Planck's constant, k_B the Boltzmann constant, and k_D the experimental rate constant of heme dissociation.

Crystal Structure Analysis. The single crystals of the Val61His fragment (Ala3−Arg84) of cytochrome Tb_5, larger than 0.5 mm × 0.5 mm × 0.3 mm, were grown using the hanging drop vapor diffusion method within 1 week from the droplet containing 10 mg/mL protein and 3.2−3.3 M phosphate (pH 7.5) at 20 °C, which is similar to the conditions used for crystallizing cytochrome Lb_5 (*5*). The crystals belong to monoclinic space group *C*2. The crystal data are shown in Table 1.

The X-ray diffraction data were collected up to 2.1 Å resolution using one crystal on a MarResearch Imaging Plate-300 detector system. The X-ray data were processed using DENZO and SCALEPACK (*35*), giving an R_{sym} of 9.0% and data completeness of 91.7%. The data collection statistics are also summarized in Table 1.

The structure was determined using the molecular replacement method (*36*) by applying the computer program Amore (*37*) of the CCP4 suite (*38*). The molecular structure of cytochrome Lb_5 at 1.5 Å resolution (*7*) was used as the search model in which all the water molecules and the side chain of Val61 were omitted. The X-ray data in the resolution range of 10.0−4.0 Å were used for the successive calculation and

Table 1: Crystal Data and Data Collection Statistics

space group	*C*2
cell dimensions	
a (Å)	70.76
b (Å)	40.43
c (Å)	39.31
β (deg)	111.88
no. of molecules per asymmetric unit	1
V_m (Å^3/Da)	2.75
no. of unique reflections	5579
R_{sym} (%)[a]	9.0 (23.2)[b]
data completeness (%)	91.7 (79.5)[b]
$\langle I/\sigma(I)\rangle$[c]	8.3 (4.0) [b]

[a] $R_{sym} = \Sigma|I - \langle I\rangle|/\Sigma I$. [b] The numbers in parentheses correspond to the data in the highest-resolution shell (2.15−2.10 Å). [c] Mean signal-to-noise ratio.

analysis of rotation function, translation function, and rigid body refinement.

The crystallographic refinement was carried out using the program package X-PLOR (*39*), and the graphics software TURBO−FRODO (*40*, *41*) was used for model fitting on a Silicon Graphics Indigo 2 workstation.

The search model transformed into the unit cell of the Val61His mutant, based on the molecular replacement solution, was initially refined as a rigid body at 2.2 Å resolution, followed by one round of atomic position and temperature factor refinement. Then the $F_o - F_c$ difference electron density map was calculated, which was used for fitting the side chain of His61. The structure was further refined for atomic positions and temperature factors with the resolution extended to 2.1 Å. The $2F_o - F_c$ and $F_o - F_c$ electron density maps were regularly calculated and used for manually rebuilding the model. The simulated annealing "omit" maps were calculated as well when necessary. In the late stage, water molecule fitting was carried out and only those water molecules with temperature factors of <50 Å^2 and hydrogen bonded to the protein atoms were included in the final model. Throughout the refinement, 10% of the X-ray data were randomly selected as the test data set used for cross validation (*42*), and the simulated annealing procedure (*43*) was performed at some points of the refinement to remove the model bias possibly introduced during the refinement.

RESULTS

Mutagenesis, Expression, and Purification of Cytochrome b_5. Mutant genes of cytochrome b_5 were successfully constructed by site-directed mutagenesis. The yield of Val61Glu and Val61Tyr is around 10 mg per liter of culture solution, while the yield of Val61Lys and Val61His is about half that of the wild type (about 15 mg/L) for these mutants are less stable and the hemes are more easily lost during the purification procedure. The purity of the proteins was confirmed by ES-MS, resulting in molecular weights of 9526.1 ± 1.9 (Val61Tyr), 9490.1 ± 3.6 (Val61Lys), 9498.9 ± 2.0 (Val61His), and 9492.3 ± 2.0 (Val61Glu). These results agreed well with the calculated values.

UV−Visible Spectrometry. As shown in Table 2, UV−visible spectra of cytochrome b_5 variants are essentially identical to that of wild-type cytochrome b_5. All oxidized forms of the proteins exhibit undistinguished absorption at 412 nm and in the far-ultraviolet region, while the reduced forms exhibit the same absorption at 424, 526, and 556 nm. The essentially identical electronic spectra of the oxidized and reduced forms of the protein variants suggest that the mutation at Val61 did not lead to significant change in the protein overall structure.

Redox Potential. The redox potential of cytochrome b_5 was sensitive to the change in the heme environment. Mutation at Val61 led to the change in redox potentials, depending upon the nature of the replacement residues (see Table 2). The potentials of Val61His and Val61Lys shift to more positive values while the potentials of Val61Tyr and Val61Glu to more negative values. These results reflect the perturbation of the heme environment by the different replacement residues.

Thermal Denaturation. Figure 2a shows the thermal denaturation curves of the wild type (WT) and the mutants of cytochrome b_5. The apparent transition temperature T_m for the transition between the folded and unfolded states was estimated from the denaturation curves in Figure 2a. An isosbestic point indicated no intermediate was observed at the equilibrium (Figure 2b); the thermal denaturation is a two-state process as described by Pace (*33*). The stabilities of cytochrome b_5 toward heat are in the following order: wild type > Val61Glu > Val61Tyr > Val61His > Val61Lys. The thermodynamic data, ΔS_m and ΔH_m, obtained during denaturation from the plot of ΔG versus temperature are summarized in Table 3.

Denaturation by Urea. Table 4 gives the results of the heme dissociation of the wild type and the mutants of cytochrome b_5 toward urea. The decreases in absorbance in the Soret band with the increasing urea concentration are shown in Figure 3. The mutant proteins are less stable than the wild type, and the half-denatured concentrations of urea estimated from denaturation curves of various mutants exhibit the same order as the T_m values of thermal denaturation. The free energy of heme denaturation by urea is the same as that of thermal denaturation, the difference being within 1.25 kJ mol^{-1}. The kinetics of urea-mediated denaturation of cytochrome b_5 were treated as a first-order reaction, producing the rate constant of the heme dissociation at different urea concentrations (see Figure 4). The rate constants increased with the increase in urea concentration, which is different from the linear relationship observed by Vergeres et al. (*12*).

Heme Transfer Reaction. The heme transfer reaction between cytochrome b_5 and myoglobin is described by a two-step procedure (eq 8).

$$\text{cytochrome } b_5 \Leftrightarrow \text{apocytochrome } b_5 + \text{heme } b \quad (8)$$

$$\text{apo-Mb} + \text{heme } b \Leftrightarrow \text{metMb}$$

In the first step, the heme dissociates from cytochrome b_5, and the second step is the recombination of the heme and apomyoglobin. It was certified that dissociation of the heme is the rate-determining step (*44*), and the whole reaction can be described as a first-order reaction. The kinetic curves of the heme transfer reaction are shown in Figure 5, and the trace can be described mathematically by eq 9

$$\Delta A_t = \Delta A_{eq}(1 - e^{-kt}) \quad (9)$$

where ΔA_t is the increase in absorbance at time t, ΔA_{eq} is the increase in absorbance at the equilibrium, and k is the

Table 2: Characterization of the Wild Type and Mutant Proteins of Cytochrome b_5

method	wild type	Val61Glu	Val61Tyr	Val61His	Val61Lys
electronic spectra, oxidized (nm)[a]	412	412	412	412	412
electronic spectra, reduced (nm)	424, 526, 556	424, 526, 556	424, 526, 556	424, 526, 556	424, 526, 556
molecular weight	9461 (9461)[c]	9492 (9491)	9526 (9526)	9499 (9499)	9490 (9490)
redox potential (mV)[b]	−10	−25	−33	11	17

[a] Absorption of the oxidized form of cytochrome b_5 in the far-ultraviolet region is not observed. [b] All the potentials listed above are referenced to SHE. The measurement error is ±3 mV. [c] Molecular weights calculated according to the amino acid composition are shown in parentheses.

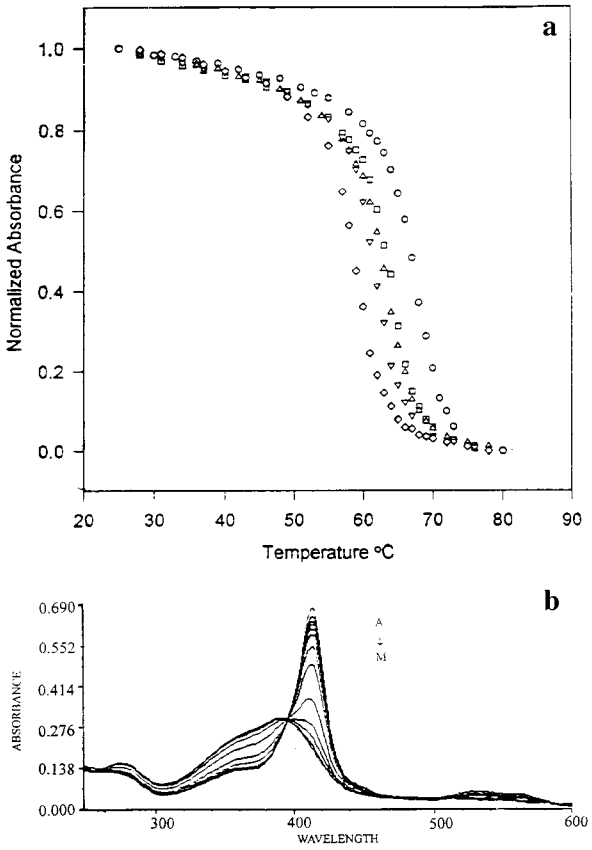

FIGURE 2: (a) Thermal denaturation curves of oxidized cytochrome b_5: (○) wild type, (□) Val61Glu, (Δ) Val61Tyr, (▽) Val61His, and (◇) Val61Lys. The data for absorbance at 412 nm were normalized (sodium phosphate, pH 7.0, 100 μM). (b) UV−visible spectra of the thermal denaturation of oxidized cytochrome b_5.

Table 3: Thermodynamic Data for Thermal Denaturation of Cytochrome b_5[a]

cytochrome b_5	T_m[b] (°C)	ΔT_m (°C)	ΔH_m (kJ/mol)	ΔS_m (J mol^{-1} K^{-1})	$\Delta(\Delta G_D^{50\%})$ (kJ/mol)
wild type	67.2	−	398	1169	−
Val61Glu	63.2	−4.0	390	1160	−4.6
Val61Tyr	62.5	−4.7	382	1137	−5.4
Val61His	61.3	−5.9	369	1127	−6.8
Val61Lys	58.5	−8.7	364	1097	−9.8

[a] Sodium phosphate, pH 7.0, 100 mM. [b] The temperature was maintained within ±0.2 °C.

rate constant of the heme transfer reaction. Data analysis was accomplished using the SigmaPlot program (Jandel Corp.). The essence of this method is to directly reflect the tightness of the heme binding to the polypeptide chain of cytochrome b_5. The time course of the increasing absorption at 406 nm is shown in Figure 5. The rate constants of heme transfer between cytochrome b_5 and myoglobin were obtained by fitting individual time courses to eq 9, and the

Table 4: Thermodynamic Data for Urea Denaturation of Cytochrome b_5[a]

cytochrome b_5	C_m (mol/L)	m_D (kJ L^{-1} mol^{-2})	$\Delta(\Delta G_D^{50\%})$ (kJ/mol)
wild type	7.7	−2.3	−
Val61Glu	6.1	−3.2	−4.4
Val61Tyr	6.0	−3.1	−5.6
Val61His	5.3	−3.3	−6.7
Val61Lys	5.2	−4.0	−10.0

[a] Sodium phosphate, pH 7.0, 100 mM.

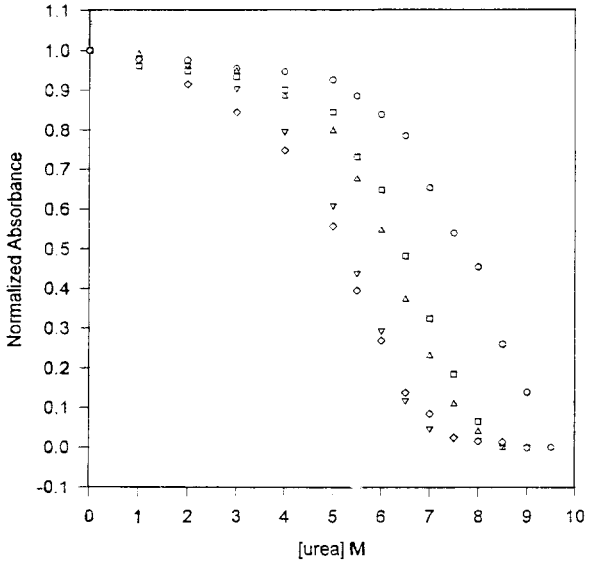

FIGURE 3: Denaturation curves of oxidized cytochrome b_5 for denaturation by urea at room temperature: (○) wild type, (□) Val61Glu, (Δ) Val61Tyr, (▽) Val61His, and (◇) Val61Lys. The data for absorbance at 412 nm were normalized (sodium phosphate, pH 7.0, 100 μM).

corresponding free energies of activation ($\Delta G_D^{\neq}$) of the heme dissociation at 20 ± 0.2 °C were calculated using eq 7. The first-order rate constants of the wild type of cytochrome b_5 and the mutant proteins were 0.25 ± 0.01 (WT), 0.42 ± 0.02 (Val61Glu), 0.93 ± 0.04 (Val61Tyr), 2.88 ± 0.01 (Val61His), and 3.88 ± 0.02 h^{-1} (Val61Lys). Compared with that of the wild type of cytochrome b_5, the corresponding activation energies for heme transfer of the four mutants at 20 ± 0.2 °C declined by 1.67−6.69 kJ/mol as shown in Table 5.

Crystal Structure of Val61His. The molecular replacement solution is shown in Table 6. Figure 6 shows the $F_o - F_c$ electron density map of the side chain of His61, calculated from the initial model in which the side chain of His61 was omitted.

The final structure refined at 2.1 Å resolution gave an *R*-factor of 19.1%. The rms deviations are 0.017 Å and 1.70° from the ideal bond lengths and bond angles, respectively.

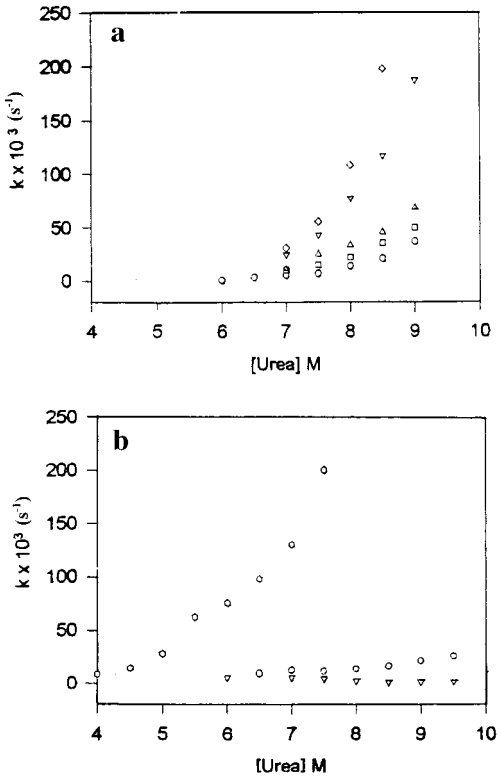

FIGURE 4: Rate constant of heme dissociation as functions of urea concentration at room temperature: (○) wild type, (□) Val61Glu, (△) Val61Tyr, (▽) Val61His, and (◇) Val61Lys. The data for absorbance at 412 nm were normalized (sodium phosphate, pH 7.0, 100 μM).

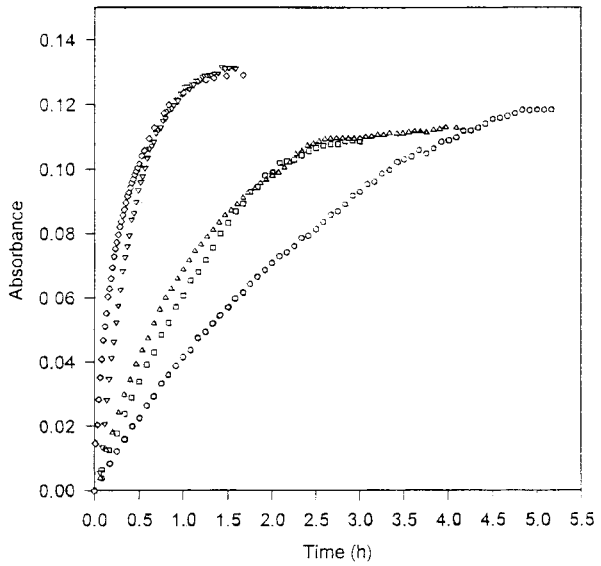

FIGURE 5: Time course of heme transfer between apomyoglobin and cytochrome b_5 measured at 406 nm: (○) wild type, (□) Val61Glu, (△) Val61Tyr, (▽) Val61His, and (◇) Val61Lys. The data for absorbance at 412 nm were normalized (sodium phosphate, pH 7.0, 100 μM).

The refinement statistics are listed in Table 7. All the conformational angles ϕ and φ of the backbone are located in the acceptable regions (93% in the most favored regions) of the Ramachandran plot (*45*), obtained by running PROCHECK (*46*). The Luzzati plot (*47*) shows that the estimated error of the atomic coordinate is approximately 0.21 Å.

Table 5: First-Order Rate Constants for Heme Transfer between Cytochrome b_5 and Apomyoglobin and the Corresponding Free Energy of Activation[a]

cytochrome b_5	k (h^{-1})	ΔG_D (kJ/mol)
wild type	0.25 ± 0.01	95.10
Val61Glu	0.42 ± 0.02	93.42
Val61Tyr	0.93 ± 0.04	91.92
Val61His	2.88 ± 0.01	89.12
Val61Lys	3.88 ± 0.02	88.41

[a] Phosphate buffer, pH 7.0, 20 ± 0.2 °C, 100 μM.

Table 6: Molecular Replacement Solution

Eularian angle (deg)	
α	43.99
β	89.35
γ	34.94
translation vector (fractional)	
Tx	0.2622
Ty	0.0000
Tz	0.2109
correlation coefficient (%)	55.9
R-factor (%)	38.2

The overall structure of Val61His is similar to that of cytochrome Lb_5 (*7*), as shown in Figure 1. The rms deviation is 0.46 Å for a total of 82 C_α atoms. The secondary structures are the same in these two structures. However, the segments of Asn16−Ser20 in the two structures exhibit different conformations, although each contains a β-turn, which can be ascribed to the intermolecular interactions that result from the particular crystal packing. In the cytochrome Lb_5 structure, this segment is somewhat flexible, with only two hydrogen bonds to the protein atoms of a symmetry-related molecule, indicated by the relatively high temperature factors (*7*). However, in the structure of the Val61His mutant, the segment of Asn16−Ser20 interacts with the protein atoms of a symmetry-related molecule, forming four hydrogen bonds, which makes it more rigid with low temperature factors. In addition, the main chain conformations of helices V are somewhat different from each other in the two structures, also related to the intermolecular interactions.

In the cytochrome Lb_5 structure, the side chain of Val61 is located in the heme-exposed edge region and points to the heme. The mutation from the small hydrophobic residue valine to a large histidine residue not only forces the side chain of this residue to point away from the heme-binding pocket to avoid the unreasonably close contacts with heme and the surrounding residues but also significantly influences the main chain conformation of the segment of Glu59−Gly62. His61 extends into the solvent, its main chain carbonyl oxygen and NE2 of the imidazole forming hydrogen bonds with two water molecules. In addition, ND1 of the imidazole is hydrogen bonded to the main chain oxygen atom of Asn57. These hydrogen bonding interactions help to stabilize the particular orientation of the His61 side chain. His61 makes van der Waals contacts with heme, and the dihedral angle between the mean plane of the heme ring and the imidazole ring of His61 is about 30°. However, the shortest distance between His61 and His63 is longer than 4.5 Å, and the two imidazole rings are almost perpendicular to each other, without the stacking interaction between them.

Panels a and b of Figure 7 show the $2F_o - F_c$ electron density map of the heme of the Val61His mutant in two

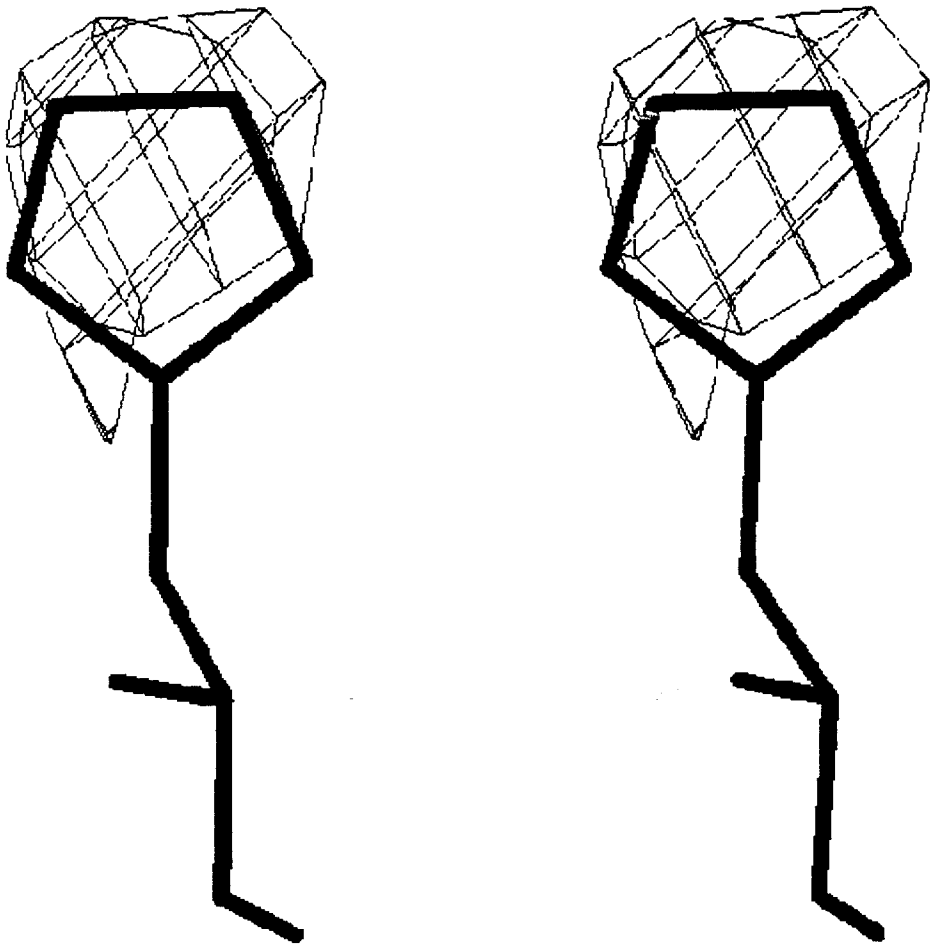

FIGURE 6: $F_o - F_c$ electron density map calculated from the initial model in which the side chain of His61 and all the water molecules were omitted. The map is contoured at 3.0σ, where σ is the rms electron density value of the map. The refined model is superimposed with the electron density. This diagram was prepared using the molecular graphics software TURBO-FRODO (*41*).

Table 7: Refinement Statistics

no. of amino acid residues	82
no. of prosthetic group	1
no. of solvent molecules	69
R-factor (%)	19.1
free *R*-factor (%)	27.0
rmsd[a]	
bond lengths (Å)	0.017
bond angles (deg)	1.70
mean temperature factors (Å^2)	
main chain	13.2
side chain	18.3
heme	13.2
solvent	33.7

[a] Root-mean-square deviation.

different views. Panels c and d show the heme and two axial ligands, His39 and His63, of the Val61His mutant, superimposed with those of cytochrome Lb_5. The remarkable feature of the Val61His mutant structure is that the coordination distances between Fe and NE2 atoms of His39 and His63 are 2.72 and 2.58 Å , respectively, about 0.6 Å longer than those in the cytochrome Lb_5 structure (*7*), suggesting that the coordination is more relaxed in this mutant than that in cytochrome Lb_5. Imposing a shorter distance restraint, as a test, does not change the results. The orientations of both the imidazole rings of the histidine ligands are also somewhat different in the two structures, approximately 10 and 20° different in χ_1 and χ_2, respectively, for His39. The two hemes themselves differ from each other as well, which can be described as a rotation about the normal of the mean plane by approximately 10°. The conformation of one of the heme propionates is conserved in the two structures, and it forms two hydrogen bonds with Ser64 (*7*); however, the other propionate exhibits a conformation slightly different from that of cytochrome Lb_5.

Three water molecules are involved in the hydrogen bonding interactions with heme propionates in the cytochrome Lb_5 structure (*7*). However, none of the three water molecules can be found in the Val61His mutant structure. On the other hand, the two water molecules hydrogen bonded to His61 in the Val61His mutant do not exist in the cytochrome Lb_5 structure.

DISCUSSION

Mutant Design Strategy. The properties and functions of cytochrome b_5 are mainly governed by two factors: structural stability and reduction potential. For the former, two kinds of stability are considered essential in the hemoproteins, namely, the stability of the secondary and tertiary structure of the protein polypeptide chain and the stability of the binding of heme to the hydrophobic pocket of the protein. For the latter, three hypotheses were proposed to be dominant for modulating the reduction potential: the hydrophobicity of the heme pocket (*48*, *49*), the hydrogen bond network

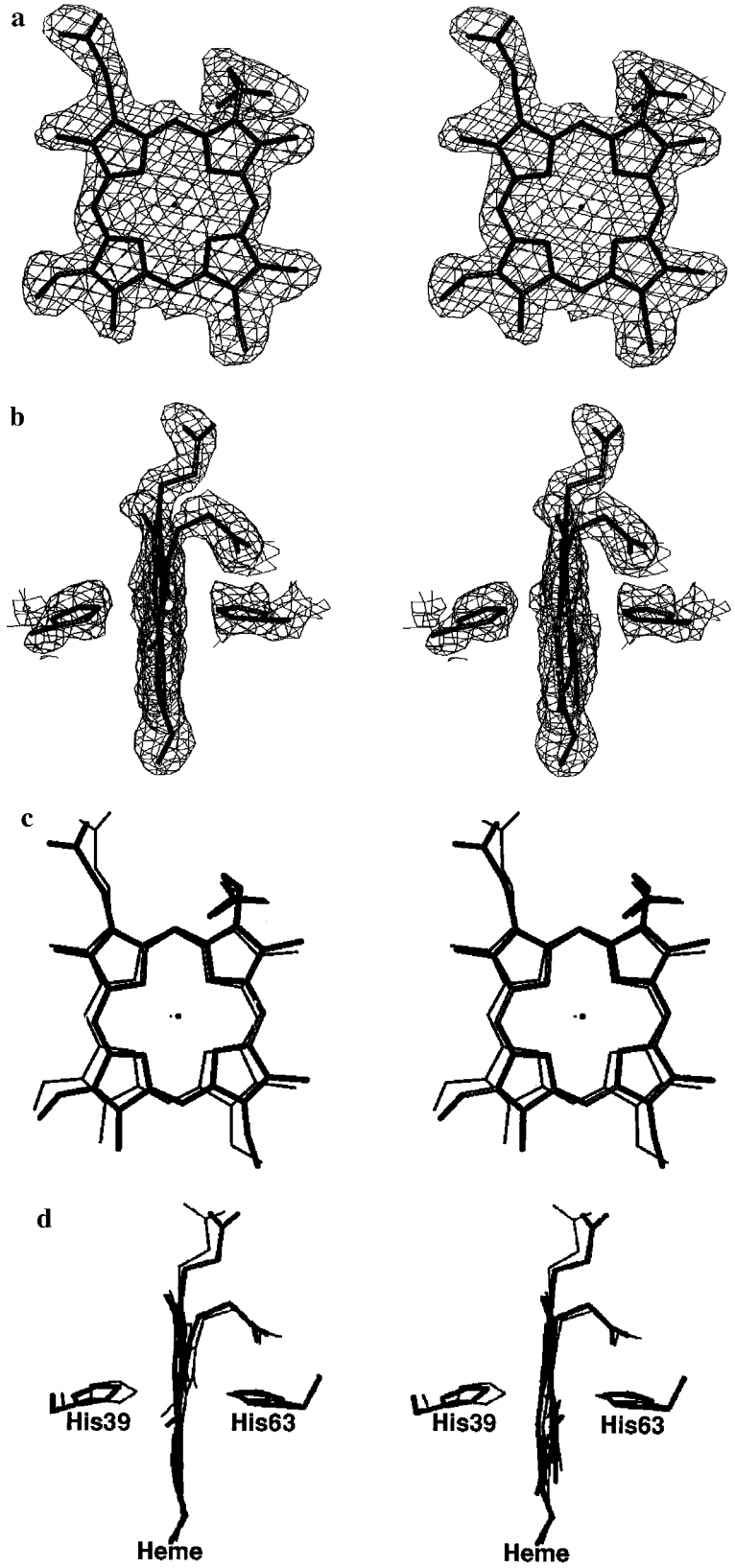

FIGURE 7: Stereoscopic diagrams prepared using the molecular graphics software TURBO-FRODO (*41*). (a) $2F_o - F_c$ electron density map of the heme of Val61His, contoured at 1.0σ. (b) $2F_o - F_c$ electron density map of heme and the axial ligands His39 and His63 of Val61His, contoured at 1.0σ. (c) Heme of Val61His, superimposed with that of cytochrome Lb_5. Val61His is shown as a thick line and cytochrome Lb_5 as a thin line. (d) Heme and His39 and His63 of Val61His, superimposed with those of cytochrome Lb_5. Val61His is shown as a thick line and cytochrome Lb_5 as a thin line.

(*50*, *51*), and the orientations of the heme plane and the axial imidazole planes as well as the binding between them (*13*, *52*).

To elucidate the roles of the Val61 of cytochrome b_5 in the protein stability, the reduction potential, and the interaction between cytochrome b_5 and its electron transfer partners,

site-directed mutagenesis is a powerful method for studying these effects. It is well understood that comparisons of closely related proteins offer the possibility of estimating the contributions of specific interactions to protein stability. The design of the Val61Tyr mutant is to test whether the bulkier residue will open a channel for water molecules to traverse the heme. The mutants Val61Glu and Val61Lys are designed to test the importance of the negatively charged surface area of cytochrome b_5 to the protein redox potential and the protein interaction. The mutant Val61His is directed to exploring the effects of the positively charged side chain and the possibility that the imidazole of His61 competes with the coordination to the heme iron against His63. Both the tyrosine and histidine substituents are also used to examine whether there is a side chain stacking interaction against the imidazole of His63.

Redox Potential. To assess whether structural changes introduced by site-directed mutagenesis have an effect on their functions (reduction potential is the most characteristic one), it is often desirable to measure the reduction potential of the redox protein and its site-directed mutants. Redox potentials of cytochrome b_5 were well studied by cyclic voltammetry and the spectroelectrochemical method in the presence of promoters (*32*, *53*, *54*), but the addition of promoters such as polylysine and Ca^{2+} and Mg^{2+} ions causes the formation of the protein−promoter complex and thus influences the electrochemical behavior of proteins at the surface of the electrode. We measured the reduction potentials using differential pulse voltammetry in the absence of promoters to rule out the effect of cations, and we believe that these results directly reflect the electric property of cytochrome b_5. The redox potentials of the mutant proteins varied in two opposite directions. The redox potentials of Val61Lys and Val61His, compared with the potential of the wild type, shift by 27 and 21 mV, respectively, in the positive direction, while the redox potentials of Val61Tyr and Val61Glu shift by 23 and 15 mV, respectively, in the negative direction. The dominant factors affecting the reduction potentials of hemoproteins generally include axially ligated residues and the heme microenvironment. Since the coordinated residues of the heme are unchanged, the changes in redox potential of cytochrome b_5 can only be attributed to the perturbation by the replacement residues of the heme environment and the conformation or orientation of the heme (*55*−*58*).

As illustrated by Matthews (*4*), in cytochrome b_5 one edge of the heme is exposed to the aqueous environment. The Val61 is situated at the rim of the heme hydrophobic pocket, its isopropyl group restricting the accessibility of water molecules to the interior of the heme pocket. In addition, cytochrome b_5 is a negatively charged protein (−10 at neutral pH), and the charge distribution on the protein surface is uneven. The heme-containing upper part of the molecule has 11 negative charges, and the negatively charged residues are mainly arranged around the heme-exposed edge; the lower part possesses one positive charge (+1). The overall macrodipole resulting from highly asymmetric charge distribution facilitates the oriented binding of charged molecules (*59*). A number of investigations (*60*−*62*) have discussed the effect of surface charge near the prosthetic group of proteins on redox potentials. It has been indicated that an increase in positive charge at the heme-exposed surface of cytochrome *c* shifts the reduction potential of hemoprotein positively, stabilizing the reduced state of the heme iron. On the contrary, a decrease in positive charge shifts the reduction potential negatively, destabilizing the reduced state of the heme iron. Here, however, in the case of the Val61 mutation of cytochrome b_5, Lys and His are positively charged residues, which reduced the negative charge density of the exposed heme edge and thus destabilized the oxidized form of the heme iron. Val61Tyr and Val61Glu maintained and strengthened the negative environment of the exposed heme edge and consequently introduced negative shifts of the redox potentials. From these results, we find out that (a) no matter whether it is a positively charged hemoprotein (cytochrome *c*) or a negatively charged hemoprotein (cytochrome b_5), the charge density (or the electrostatic potential) at the exposed heme region regulates the reduction potential of the heme iron and (b) no matter whether it is an "exogenous" charged species such as Mg^{2+} ion (*54*) and polylysine (*53*) or an "endogenous" charged group such as lysine, glutamic acid, and histidine (this study), it exerts influence on the reduction potential of the heme iron.

During the preparation of this paper, we noticed that Rivera et al. (*15*) recently reported their study on polylysine-promoted cyclic voltammetry of outer membrane cytochrome b_5 and dimethylpropionate cytochrome b_5. They found that a negative shift in the reduction potential of the cytochrome b_5 Val45Leu/Val61Leu double-site mutant was due to an increased dielectric constant in the heme microenvironment. In addition, the crystal structure of the Val61His mutant shows that mutation from Val61 to His61 does reduce the hydrophobicity of the heme pocket. Moreover, we also studied mutants of cytochrome b_5 at position of Phe35 (*11*), and it is demonstrated that perturbation of the hydrophobicity of the heme pocket is also one of the most important factors determining the redox potential of the heme proteins. On the basis of the observations described above, we believe that the electrostatic potential in the heme-exposed region and the hydrophobicity of the heme pocket control and/or modulate the reduction potential of the positive heme

Protein Stability. In our study, the hydrophobic residue Val61 was mutated to four larger and/or polar residues to assess the contribution of Val61 to the structural stability and properties of cytochrome b_5. Denaturation of cytochrome b_5 by heat and denaturants such as urea was usually used to measure the stability of cytochrome b_5 and its variants (*11*, *63*, *64*). As shown in Tables 3 and 4, the stabilities of cytochrome b_5 determined by both heat and urea are displayed in a decreasing order: wild type > Val61Glu > Val61Tyr > Val61His > Val61Lys. The crystal structure of Val61His shows that its secondary and tertiary structures do not obviously change, compared with those of cytochrome Lb_5, implying that the denaturation is probably not related to the stability of the overall structure of cytochrome b_5. On the other hand, it was certified that the denaturation of cytochrome b_5 toward heat and urea is accompanied by heme dissociation. There are several factors, including the hydrophobic effect and hydrogen bond, salt bridge, and van der Waals interaction, contributing to the stability of the protein. Among these, hydrophobic interaction is considered to be a dominant force. It was reported that the hydrophobic effects contribute approximately 8 kJ/mol per residue, on average, to the free energy of protein folding at room temperature

(*65*). Meanwhile, mutagenesis studies with phage T4 lysozyme have shown that single hydrogen bond typically contributes 4.18−6.27 kJ/mol to protein stability (*26*).

First of all, let us consider the side chain volume of the residues being substituted for Val61. The increases in the volume of the mutants are 13 (Val61Glu), 62 (Val61Tyr), 26 (Val61His), and 30 Å^3 (Val61Lys) (*65*). It seems that the volume increase of the replacement residues makes a contribution to the instability of the heme binding, but the Val61Tyr mutant does not conform to this rule. The crystal structure of the Val61His mutant shows that the side chain of His61 points away from the heme-binding pocket and extends into the solvent. Although the exact three-dimensional structures of the other three mutants have not yet been determined, the preliminary computer modeling of them was performed, based on the crystal structure of the Val61His mutant, by replacing the side chain of residue 61, manually adjusting the side chain conformation, and examining their environment. The computer-built models show that the bulky or long side chains of glutamic acid, tyrosine, and lysine are impossible to be buried in the heme pocket. To avoid unreasonably close contacts, it is necessary for these side chains to extend into solvent. The C_β and C_γ atom positions of these three mutants are similar to those of Val61His, and the remaining parts of the side chains of this residue are located completely out of the heme-binding pocket. Therefore, the increases in the side chain volume will not lead to much change in the heme environment or the heme-binding stability.

As mentioned above, the conserved residue Val61 is located at the rim of the heme hydrophobic pocket, with a shortest distance of about 3.9 Å to the heme atom, and its isopropyl group might act as a "gate" restricting the access of water molecules to the heme pocket. The crystal structure of the Val45Leu/Val61Leu double-site mutant of outer membrane mitochondrial cytochrome b_5 was recently reported (*15*) and compared with the corresponding wild-type structure (*8*), which shows that the isobutyl groups of Leu45 and Leu61 point away from the heme group, thus resulting in a "channel" that traverses the heme cavity. In our Val61His mutant structure, the main chain of the segment of Glu59−Gly62 moves toward the heme, and the position of one of the C_γ atoms of Val61 of cytochrome Lb_5 is not occupied, suggesting that the gate formed by Val61 could be considered partially opened in the Val61His mutant structure. On the other hand, the bulky imidazole ring swings away to the site, making a dihedral angle of about 30° with the heme mean plane and the shortest distance to the heme atoms being about 3.5 Å, which implies that the imidazole ring of His61 might form a new gate. Therefore, the microenvironment of heme and the accessibility of water to the heme pocket are slightly disturbed.

Furthermore, it is indicated that the heme environment could be altered by changing the polarity of the side chain located near the heme or changing the extent of solvent exposure of the heme. Increases in the positive charge density of bovine pancreatic trypsin inhibitor and phage T4 lysozyme at solvent-exposed positions decreased the stability by 2.09−4.18 kJ/mol (*66*−*68*), and in the heme protein, alteration of the charge density near the exposed heme area causes more severe effect on protein stability (4.18−8.36 kJ/mol). The stabilities of the four mutants of cytochrome b_5 are reduced with the decrease in the negative charge and the increase in the positive charge of the mutated residue, implying that the "electrostatic potential" is probably one of the main factors influencing the heme binding stability. Nevertheless, in the three-dimensional structure of cytochrome Lb_5 (*69*), it is noted that one of the propionates of the heme group is completely buried in the heme pocket, and the other propionate is located entirely out of the heme pocket. There is a hydrogen bond network formed by carboxyl oxygen atoms of both propionates, Val61, Ser64, and three water molecules around the exposed heme edge. This hydrogen bond network helps to stabilize the heme binding. However, the hydrogen bond network can easily be destroyed by the introduction of the larger and charged residues, resulting in the changes in redox potentials and the destabilization of the hemoproteins (*9*, *61*). The crystal structure of the Val61His mutant does indicate that this hydrogen bond network no longer exists, suggesting that this part of the protein molecule is disturbed. It is obvious that the hydrogen bond network is another principal contributor to the stability of cytochrome b_5.

Apomyoglobin was often employed as a trap to test the tightness of heme attaching to the peptides of cytochrome b_5 since it comparatively traps heme so fast that the heme dissociation from the other hemoproteins is the rate-determining step (*12*, *70*). The ratio of the rate constants is 1:2:4:12:16 (WT:Val61Glu:Val61Tyr:Val61His:Val61Lys), implying that the polypeptide chain of wild-type cytochrome b_5 binds the heme 16−2 times as tightly as the mutants do. The heme binding ability examined by the heme transfer reaction is virtually consistent with those by thermal and urea-mediated denaturation as discussed above, which further confirm that the denaturation of cytochrome b_5 toward heat and urea is mainly a heme dissociation process. Probably, the more relaxed coordination of two axial ligands with iron ion, indicated by the longer coordination distances, in the Val61His mutant than in those in cytochrome Lb_5 (*7*) can account for these results. Since the crystal structure of wild-type cytochrome Tb_5 has not yet been determined, this conclusion will not be drawn until the wild-type structure analysis is completed. Meanwhile, if we compare the results with those from heme transfer reactions of Tyr74Lys (*12*) and Glu44Ala, Glu56Ala, and Glu44Ala/Glu56Ala mutants of cytochrome b_5 (*10*), the heme binds the apo form of wild-type cytochrome b_5 about 6-fold more tightly than the Tyr74Lys mutant does, while being only slightly different from the Glu44Ala, Glu56Ala, and Glu44Ala/Glu56Ala mutants (*10*). This is because the side chains of these mutants are located on the protein's surface and do not greatly affect the heme stability. On the contrary, the mutant proteins varied at the Phe35 of cytochrome b_5 induce the decrease in the heme stability since Phe35 is adjacent to the heme in the hydrophobic pocket, and NMR results show that it has close contact with the heme (*71*).

CONCLUSION

The results obtained in this study provide further insight into the role of Val61 of cytochrome b_5. Val61 is positioned at the rim of the heme hydrophobic pocket and is proximate not only to the heme ring but also to the heme propionates. The properties of the mutants at Val61 of cytochrome b_5 are closely related to the properties of the substituting

residues. Val61His and Val61Lys introduce positive charges, while Val61Glu and Val61Tyr bring a negatively charged or a polar residue to the heme-exposed edge. Therefore, the mutations at Val61 change the electrostatic potential of the microenvironment of the exposed heme edge and the hydrophobicity of the heme-binding pocket, thus consequently giving rise to the change in the redox potential of cytochrome b_5. The crystal structure of the Val61His mutant shows that the imidazole side chain of His61 points away from the heme-binding pocket and extends into the solvent, the coordination distances from Fe to NE2 atoms of two axial ligands are 0.6 Å longer than those in wild-type cytochrome Lb_5, and the hydrogen bond network of cytochrome Lb_5 involving Ser64, the carbonyl oxygen of Val61, the heme propionates, and three water molecules is destroyed. Hence, we can reach the conclusion that the electrostatic potential around the Val61 area is an important factor in modulating the redox potential, while the hydrogen bond network around the exposed heme edge also contributes to the properties and stability of cytochrome b_5.

ACKNOWLEDGMENT

We thank Ms. Yong-Zhen Xu of the Shanghai Institute of Organic Chemistry for the ES-MS study. We express our gratitude to Prof. Li-wen Niu and Dr. Xue-yong Zhu of the University of Science and Technology of China for their support and help with the X-ray data collection.

REFERENCES

1. Hultquist, D. E., Sannes, L. G., and Juckett, D. A. (1984) *Curr. Top. Cell. Regul. 24*, 278−300.
2. Strittmatter, P., Spatz, L., Corcoran, D., Rogers, M. J., Setlow, B., and Redline, R. (1974) *Proc. Natl. Acad. Sci. U.S.A. 71*, 4565−4569.
3. Cohen, B., and Estabrook, R. W. (1971) *Arch. Biochem. Biophys. 143*, 54−65.
4. Matthews, F. S. (1985) *Prog. Biophys. Mol. Biol. 45*, 1−56.
5. Mathews, F. S., Levine, M., and Argos, P. (1972) *J. Mol. Biol. 64*, 449−464.
6. Mathews, F. S., Argos, P., and Levine, M. (1971) *Cold Spring Harbor Symp. Quant. Biol. 36*, 387−395.
7. Durley, R. C. E., and Mathews, F. S. (1996) *Acta Crystallogr. D52*, 65−76.
8. Rodriguez-Maranon, M. J., Qiu, F., Stark, R. E., White, S. P., Zhang, X., Foundling, S. I., Rodriguez, V., Schilling, C. L., Bunce, R. A., and Rivera, M. (1996) *Biochemistry 35*, 16378−16390.
9. Lee, K. B., Eunsoon, J., Lar Mar, G. N., Rezzano, I. N., Pandey, R. K., Smith, K. M., Walker, F. A., and Buttlaire, D. H (1991) *J. Am. Chem. Soc. 113*, 3576−3583.
10. Sun, Y. L., Xie, Y., Xiao, G. T., and Huang, Z. X. (1996) *Protein Eng. 9*, 555−558.
11. Yao, P., Xie, Y., Wang, Y. H., Sun, Y. L., Huang, Z. X., Xiao, G. T., and Wang, S. D. (1997) *Protein Eng. 10*, 575−581.
12. Vergeres, G., Chen, D. Y., Wu, F. F., and Waskell, L. (1993) *Arch. Biochem. Biophys. 305*, 231−241.
13. Sarma, S., Dangi, B., Yan, C. H., DiGate, R. J., Banville, D. L., and Guiles, R. D. (1997) *Biochemistry 36*, 5645−5657.
14. Funk, W. D., Lo, T. P., Mauk, M. R., Brayer, G. D., MacGillivray, R. T. A. M., and Mauk, A. G. (1990) *Biochemistry 29*, 5500−5508.
15. Rivera, M., Seetharaman, R., Girdhar, D., Wirtz, M., Zhang, X. J., Wang, X. Q., and White, S. (1998) *Biochemistry 37*, 1485−1494.
16. Salemme, F. R. (1976) *J. Mol. Biol. 221*, 1453−1460.
17. Northrup, S. H., Thomassm, K. A., Miller, C. M., Barker, P. D., Eltis, L. D., Guillemette, J. G., Inglis, S. C., and Mauk, A. G. (1993) *Biochemistry 32*, 6613−6623.
18. Bodman, S. B., Schuler, M. A., Jollie, D. R., and Sligar, S. G. (1986) *Proc. Natl. Acad. Sci. U.S.A. 83*, 9443−9447.
19. Sligar, S. G., and Egeberg, K. D. (1987) *J. Am. Chem. Soc. 109*, 7896−7897.
20. Ng, S., Smith, M. B., Smith, H. T., and Millett, F. (1977) *Biochemistry 16*, 4975−4978.
21. Bonfils, C., Balny, C., and Maurel, P. (1981) *J. Biol. Chem. 256*, 9457−9465.
22. Poulos, T. L., and Mauk, A. G. (1983) *J. Biol. Chem. 258*, 7369−7373.
23. Rogers, K. K., Pochapsky, T. C., and Sligar, S. G. (1988) *Science 240*, 1657−1659.
24. Willie, A., McLean, M., Liu, R. Q., Hilgen-Willis, S., Saunders, A. J., Pielak, G. J., Sligar, S. G., Durham, B., and Millet, F. (1993) *Biochemistry 32*, 7519−7525.
25. Creighton, T. E. (1983) *Biophysics 22*, 49−58.
26. Alber, T., Sun, D. P., Nye, J. A., Machmore, D. C., and Matthews, B. W. (1987) *Biochemistry 26*, 3754−3758.
27. Guillemette, J. G., Barker, P. D., Eltis, L. d., Lo, T. P., Smith, M., Brayer, G. D., and Mauk, A. G. (1994) *Biochimie 76*, 592−604.
28. Mauk, A. G., Mauk, M. R., Moore, G. R., and Northrup, S. H. (1995) *J. Bioeng. Biomembr. 27*, 311−330.
29. La Mar, G. N., Tio, H., and Krishnamoorthi, R. (1984) *J. Am. Chem. Soc. 106*, 6395−6401.
30. Zoller, M. J., and Smith, M. (1983) *Methods Enzymol. 100*, 458−500.
31. Newbold, R. G., Hewson, R., and Whitford, D. (1992) *FEBS Lett. 314*, 419−424.
32. Qian, W., Zhuang, J. H., Wang, Y. H., and Huang, Z. X. (1998) *J. Electroanal. Chem. 447*, 187−189.
33. Pace, C. N. (1986) *Methods Enzymol. 131*, 266−280.
34. Matthews, C. R. (1987) *Methods Enzymol. 154*, 498−511.
35. Otwinowski, Z., and Minor, W. (1997) *Methods Enzymol. 276*, 307−326.
36. Rossman, M. G. (1972) in *The Molecular Replacement Method* (Rossman, M. G., Ed.) pp 4−24, Gordon and Breach, New York.
37. Navaza, J. (1994) *Acta Crystallogr. A50*, 157−163.
38. Collaborative Computational Project, Number 4 (1994) *Acta Crystallogr. D50*, 760−763.
39. Brünger, A. T. (1993) *X-PLOR (version 3.1). Manual of a system for X-ray Crystallography and NMR*, Yale University Press, New Haven, CT.
40. Jones, T. A. (1985) *Methods Enzymol. 115*, 157−171.
41. Roussel, A., and Cambillau, C. (1991) *TURBO-FRODO. Silicon Graphics Geometry Partners Dictionary*, p 86, Silicon Graphics Inc., Mountain View, CA.
42. Brunger, A. T. (1992) *Nature 335*, 472−475.
43. Brunger, A. T., Kurijian, J., and Karplus, M. (1987) *Science 235*, 458−460.
44. Adams, P. A. (1977) *Biochem. J. 163*, 153−158.
45. Ramachandran, G. N., and Sasasekharan, V. (1968) *Adv. Protein Chem. 28*, 283−473.
46. Laskowski, R. A., McArthur, M. W., Moss, D. S., and Thornton, J. M. (1993) *J. Appl. Crystallogr. 26*, 283−291.
47. Luzzati, P. V. (1952) *Acta Crystallogr. 5*, 802−810.
48. Kassner, R. J. (1972) *Proc. Natl. Acad. Sci. U.S.A. 69*, 2263−2267.
49. Stellwagen, E. (1978) *Nature 275*, 73−74.
50. Quinn, R., Mercer-Smith, J., Burstym, J. N., and Valentine, J. S. (1984) *J. Am. Chem. Soc. 106*, 4136−4144.
51. Goodin, D. B., and McRee, D. E. (1993) *Biochemistry 32*, 3313−3334.
52. Sarma, S., DiGate, R. J., Goodin, D. B., Miller, C. J., and Guiles, R. D. (1997) *Biochemistry 36*, 5645−5657.
53. Rivera, M., Wells, M. A., and Walker, F. A. (1994) *Biochemistry 33*, 2161−2170.
54. Wang, Y. H., Cui, J., Sun, Y. L., Yao, P., Zhuang, J. H., Xie, Y., and Huang, Z. X. (1997) *J. Electroanal. Chem. 428*, 39−45.
55. Mashiko, T., Reed, C. A., Haller, K. J., Kastner, M. E., and Scheidt, W. R. (1981) *J. Am. Chem. Soc. 103*, 5758−5767.

56. Moore, G. R., and Williams, R. J. P. (1977) *FEBS Lett. 79*, 229−232.
57. Moore, G. R., Harris, D. E., Leitch, F. A., and Pettigrew, G. W. (1984) *Biochim. Biophys. Acta 764*, 331−342.
58. Geiger, D. K., Lee, Y. J., and Scheidt, W. R. (1984) *J. Am. Chem. Soc. 106*, 6339−6343.
59. Qian, W., Sun, Y.-L., Wang, Y.-H., Zhuang, J.-H., Xie, Y., and Huang, Z.-X. (1998) *Biochemistry 37*, 14137−14150.
60. Caffrey, M. S., and Cusanovich, M. A. (1991) *Arch. Biochem. Biophys. 285*, 227−230.
61. Caffrey, M. S., Daldal, F., Holden, H. M., and Cusanovich, M. A. (1991) *Biochemistry 30*, 4119−4125.
62. Caffrey, M. S., and Cusanovich, M. A. (1994) *Biochim. Biophys. Acta 1187*, 277−288.
63. Sugiyama, T., Miura, R., and Yamano, T. (1980) *Biochem. Biophys. Res. Commun. 97*, 22−27.
64. Pfeil, W., and Bendzko, P. (1980) *Biochim. Biophys. Acta 626*, 73−78.
65. Caffrey, M. S. (1994) *Biochimie 76*, 622−630.
66. Pakula, A. A., Vincent, B. Y., and Sauer, R. T. (1986) *Proc. Natl. Acad. Sci. U.S.A. 83*, 8829−8833.
67. Wagner, G., Kalb, A. J., and Wuthrich, K. (1979) *Eur. J. Biochem. 95*, 249−253.
68. Grutter, M. G., and Matthews, B. W. (1982) *J. Mol. Biol. 154*, 525−535.
69. Matthews, B. W. (1993) *Annu. Rev. Biochem. 63*, 139−160.
70. Rose, M. Y., and Olson, J. S. (1983) *J. Biol. Chem. 258*, 4298−4303.
71. Yao, P., Wang, Y. H., Xie, Y., and Huang, Z. X. (1998) *Chin. Sci. Bull. 43*, 214−217.
72. Evans, S. V. (1993) *J. Mol. Graphics 11*, 134−138.

BI990893B